Available online at www.CivileJournal.org

Civil Engineering Journal

(E-ISSN: 2476-3055; ISSN: 2676-6957)

Vol. 8, No. 12, December, 2022

Some Approaches to the Prediction of Permeability Parameters in a Finite Element Program for Early Warning

Krairoj Mahannopkul [1], Chollada Kanjanakul [2*]

[1] *Department of Teacher Training in Civil Engineering, King Mongkut's University of Technology North Bangkok, Thailand.*

[2] *Department of Civil Engineering, The Research Unit of Technology and Innovation on Civil Engineering (RICE), Rajamangala University of Technology Srivijaya, Nakhon Si Thammarat, Thailand.*

Received 01 October 2022; Revised 14 November 2022; Accepted 23 November 2022; Published 01 December 2022

Abstract

Recently, landslides often occurred in natural soil slopes in the tropical region, which correlate with the rainy season. Rainfall infiltration leads to groundwater level fluctuations. The increased positive pore-water pressures due to rainfall influence have affected the properties and behavior of the unsaturated soil slope. In this research, the Finite Element Method of SEEP/W and SLOPE/W analyzes the factor safety of the slope affected by pore water pressure change due to rainfall. The Soil Water Characteristic Curve (SWCC) and Hydraulic Conductivity function were obtained from sieve analysis and Atterberg's limit. In addition, unsaturated soil properties from the UNSODA code are estimated based on grain-size distribution using the SWRC program. The study area is in Khanom District, southern Thailand. The results show that the soil slope at the site became unstable on November 18, 2021, with F.S. = 1.0, which agrees well with the date of the disaster. In conclusion, the slope stability analysis without the parameters from the unsaturated soil hydraulic database (UNSODA) leads to the F.S. value being higher than the actual value, and the alarm estimation would be inaccurate.

Keywords: Soil Water Characteristic Curve (SWCC); Unsaturated Soil Hydraulic Database (UNSODA); Early Warning; Slope Stability Analysis; Rainfall Infiltration.

1. Introduction

Landslides in mountainous areas during heavy rainfall can result in the loss of lives and properties. Various geotechnical studies have applied an early warning system for landslides to mitigate the risk [1]. For example, Yang et al. [2] established the rainfall threshold for landslide activity in Dazhou, China, and used the parameter combined with the intraday rainfall to represent the rainfall condition. Kardani et al. [3] used the finite element method (FEM) to simulate slope stability and generate synthetic data for the training of the optimized machine learning methods (OML) that were employed to predict slope stability on the testing dataset. Zheng et al. [4] proposed the triangular fuzzy number and the analytic hierarchy process method with GIS that effectively predicted the distribution of geo-hazard risk in the study region along the Chengdu-Kunming railway, southwestern China, generated from case studies within the past ten years.

In a particular region, rainfall is the main factor for slope failures, and rainfall thresholds are the significant parameter in forecasting the landslide probability [5, 6]. Many researchers have shown great potential in predicting landslide and debris flow events by machine learning with time-series data processing methods based on continuous rainfall records. Zhao et al. [7] used this approach to predict debris flow events based on continuous rainfall records from five rain gauges in the catchment. Jiang et al. [8] presented the probabilistic rainfall thresholds for debris flow occurrences under specific rainfall conditions by applying a Bayesian approach based on the Wenchuan earthquake.

* Corresponding author: chollada.k@rmutsv.ac.th, chollada-ka@hotmail.com

http://dx.doi.org/10.28991/CEJ-2022-08-12-014

Soil-water characteristic curves (SWCC) are one of the fundamental elements used to analyze slope seepage and stability under rainfall conditions. It plays a vital role in reflecting the hydro-mechanical behavior of unsaturated soils [9, 10]. In addition, the SWCC describes a relationship between the amount of soil water and suction drawn on a curve. Many researchers have tried to create SWCC equation models for the complete modeling of graph analysis. Hamdany et al. [11], for example, developed the field SWCC in Singapore by combining the measured in-situ soil suction from the NTU osmotic tensiometer with the measured in-situ water content from the moisture sensor. While Wang et al. [12] used a Bayesian approach to probabilistically characterize SWCC and unsaturated hydraulic conductivity, systematically combining available test data from practical engineering measurements. Furthermore, engineers have constantly tried to use particle-size distribution data and improve mathematical models for the estimation of SWCC (e.g., Dafalla et al. [13], Wang et al. [14], and Zhou et al. [15]).

Rainfall-induced landslides in Nakhon Si Thammarat province, Thailand, caused casualties and damage to properties. The SWCC is a crucial prerequisite for analyzing the process of landslides in unsaturated soils [16]. This paper aimed to develop SWCC by the basic physical properties data from soil sampling and data in the Unsaturated Soil Database (UNSODA). Monthly rainfall measurements were used in finite element programs to compute the factors of safety in the soil slope.

2. Description of Studied Site

The study area was a mountain slope near the sea, Khanom District, Nakhon Si Thammarat Province, Southern Thailand, position 9°07'27.9"N 99°53'05.0"E, as shown in Figure 1; the amount of rainfall is shown in Figure 2. The total number of rainy days in 2021 is 84, with a total annual rainfall of 1,189.1 mm in the area.

Figure 1. Map and aerial photos of the study site

Soil properties at the site were examined by Sieve Analysis, Atterberg Limit, and Specific Gravity, as shown in Table 1. A summary of the basic properties, which can be classified according to the Unified Soil Classification system as Silty Sand (S.M.).

Table 1. The basic properties of soil

Test	Properties		
	Top	**Middle**	**Bottom**
Grain size distribution	Clay/silt = 4.80%, Sand = 89.04 %, gravel = 6.00%	Clay/silt = 4.40%, Sand = 79.40 %, gravel = 16.00%	Clay/silt = 5.20%, gravel = 18.40% gravel = 18.40%
Specific gravity	Gs = 2.69	Gs =2.67	Gs =2.70
Atterberg's Limits	LL = 28.43% PL =26.66 % PI = 1.31%	LL = 41.00% PL =40.13 % PI = 0.87%	LL = 38.93% PL =37.90 % PI = 1.03%
USCS soil Type	SM-Silty Sand	SM-Silty Sand	SM-Silty Sand

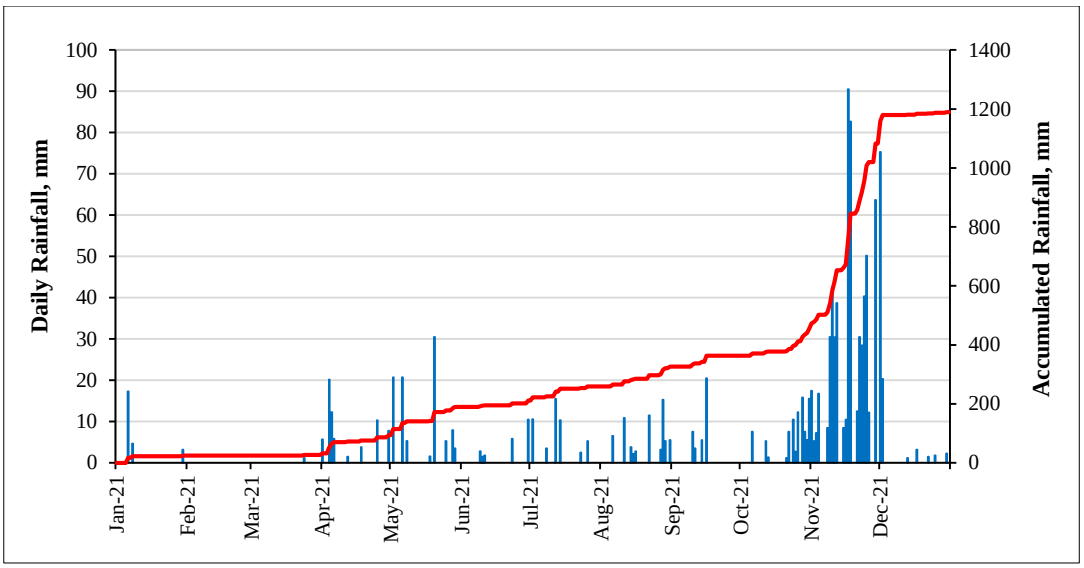

Figure 2. Variation of daily rainfall in 2021

3. Research Methodology

Four stages, as shown in Figure 3. were conducted in this research: (i) Preparation of slope models for GeoStudio analysis using geotechnical laboratory data and traditional survey; (ii) Comparison between soil sampling and unsaturated soil hydraulic database (UNSODA); (iii) The use of permeability behaviors and rainfall intensity to calculate pore water pressure variation by SEEP/W; (iii) Calculation of factors of safety of the unsaturated slope by SLOPE/W. These are described in more detail in "Determination of site-specific SWCC from original tests in UNSODA" through to the "Estimate fitting parameters from SWRC program" section, thus:

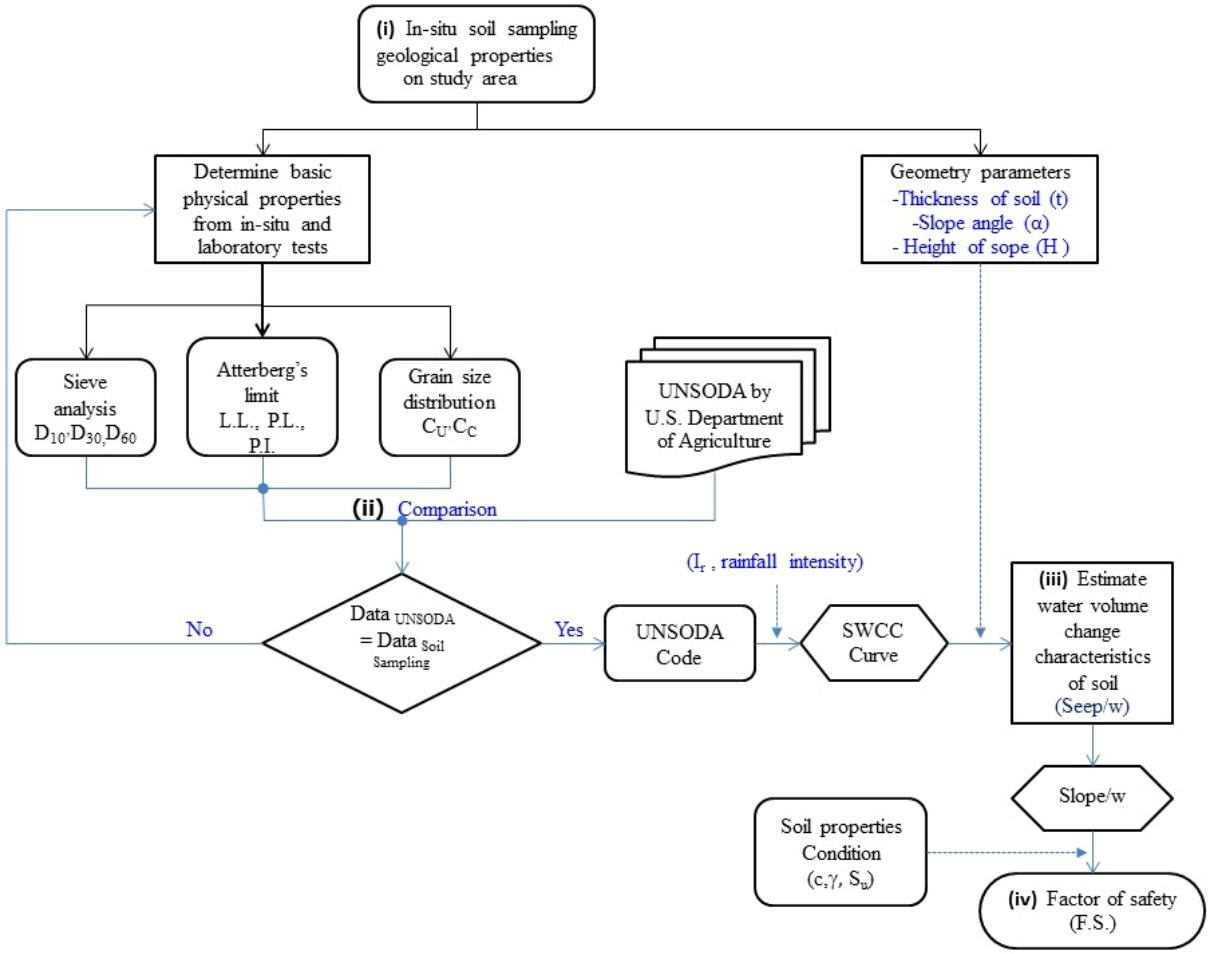

Figure 3. Process for analysis, fitting, and verification

3.1. Determination of Site-Specific SWCC from Original Tests in UNSODA

UNSODA is a database with water retention and saturated and unsaturated hydraulic conductivity. The author describes a method to determine the UNSODA code by comparing basic properties results from physical laboratory parameters. Grain size distribution curves performed on samples collected from Top, Middle, and Bottom positions in the study area revealed that each soil position clearly exhibits different particle sizes and physical characteristics. Due primarily to geological changes. As time passed, the granite slope (gr) shown in Figure 1 decomposed and degraded to silt and sand. These soil samples can be classified as silty sand (S.M.) under the unified soil classification system (USCS).

As shown in Figure 4 and Table 2, Topsoil properties Liquid Limit (L.L.) obtained from Atterberg limits laboratory testing (ASTM D 4318-04) are 28.43, Plastic limit (P.L.); 26.66, and 1.31, Plastic Index (P.I.). The S.M. part from Middle and Lower positions properties Liquid Limit (L.L.) obtained from Atterberg limits laboratory testing are 41.00 and 38.93, Plastic limit (P.L.); 40.13 and 37.90, and 0.87 and 1.03, Plastic Index (P.I.). For comparison of laboratory physical parameter determinations with soil data from the UNSODA code, e.g., top-level soil sample. Soil properties in mm such that 10%, 30%, and 60% of particles are finer than this size (D_{10}, D_{30}, and D_{60}) from Sieve Analysis laboratory testing are 0.12, 0.35, and 0.90. The coefficient of uniformity (C.U.) is 7.5 and 1.13, and the coefficient of curvature (CC). For Middle and bottom lower-level soil samples, In the soil properties study area, D_{10}, D_{30}, and D_{60}) from Sieve Analysis laboratory testing are 0.13, 0.62, and 2.1 (Middle position) and 0.14, 0.60, and 2.30 (Bottom position). The coefficient of uniformity (C.U.) is 16.15 for the middle and 16.43 for the bottom position, and the coefficient of curvature (CC) is 1.41 for the middle and 1.12 for the bottom position.

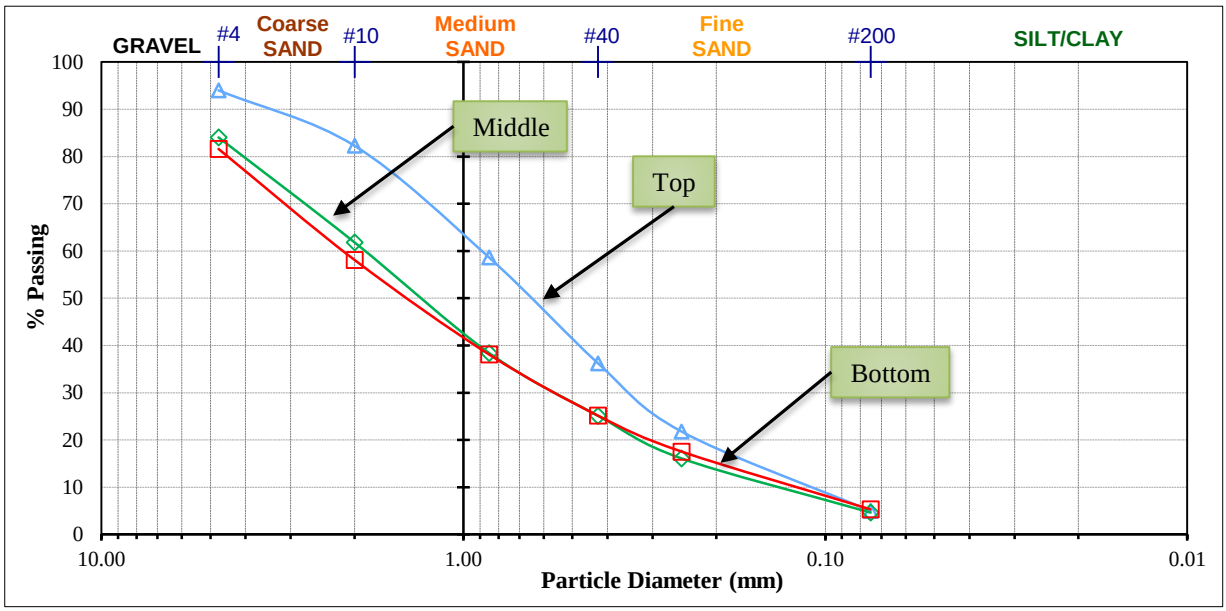

Figure 4. Particle-Size Distribution Data

Table 2. The comparison was between soil sampling SM and UNSODA 1090, UNSODA 4251

Sample	Position Top	UNSODA 1090 (Loamy Sandy)	Position Middle	UNSODA 4251 (Loamy Sandy)	Position Bottom	UNSODA 4251 (Loamy Sandy)
D_{10}	0.1200	0.1200	0.1300	0.1400	0.1400	0.1400
D_{30}	0.3500	0.3700	0.6200	0.6300	0.6000	0.6300
D_{60}	0.9000	0.9500	2.1000	2.3000	2.3000	2.3000
C_u	7.5000	7.9200	16.1538	16.4290	16.4300	16.4290
C_c	1.1300	1.2000	1.4081	1.2326	1.1200	1.2326
	n	5.0000		5.0000		5.0000
	df	3.0000		3.0000		3.0000
	R^2(%)	98.1665		98.5408		99.8642

The particle size distribution data can be used to estimate the SWCC as well, e.g., Minasny et al. [17], Chiu et al. [18], and Wang et al. [19]. As shown in Table 2, the results from the topsoil were similar to the UNSODA 1090, with an R^2 value of 0.9817. The samples from middle and lower positions were similar to the UNSODA 4251, with R^2 values of 0.9854 and 0.9986.

3.2. Estimate Fitting Parameters from SWRC Program

Employing permeability data from UNSODA 1090 and UNSODA 4251 in general report U.S. Department of Agriculture, soil water retention curve (SWRC) program was used to calculate principal parameters such as the volumetric water content at saturated and residual conditions and constant parameter (Figure 5).

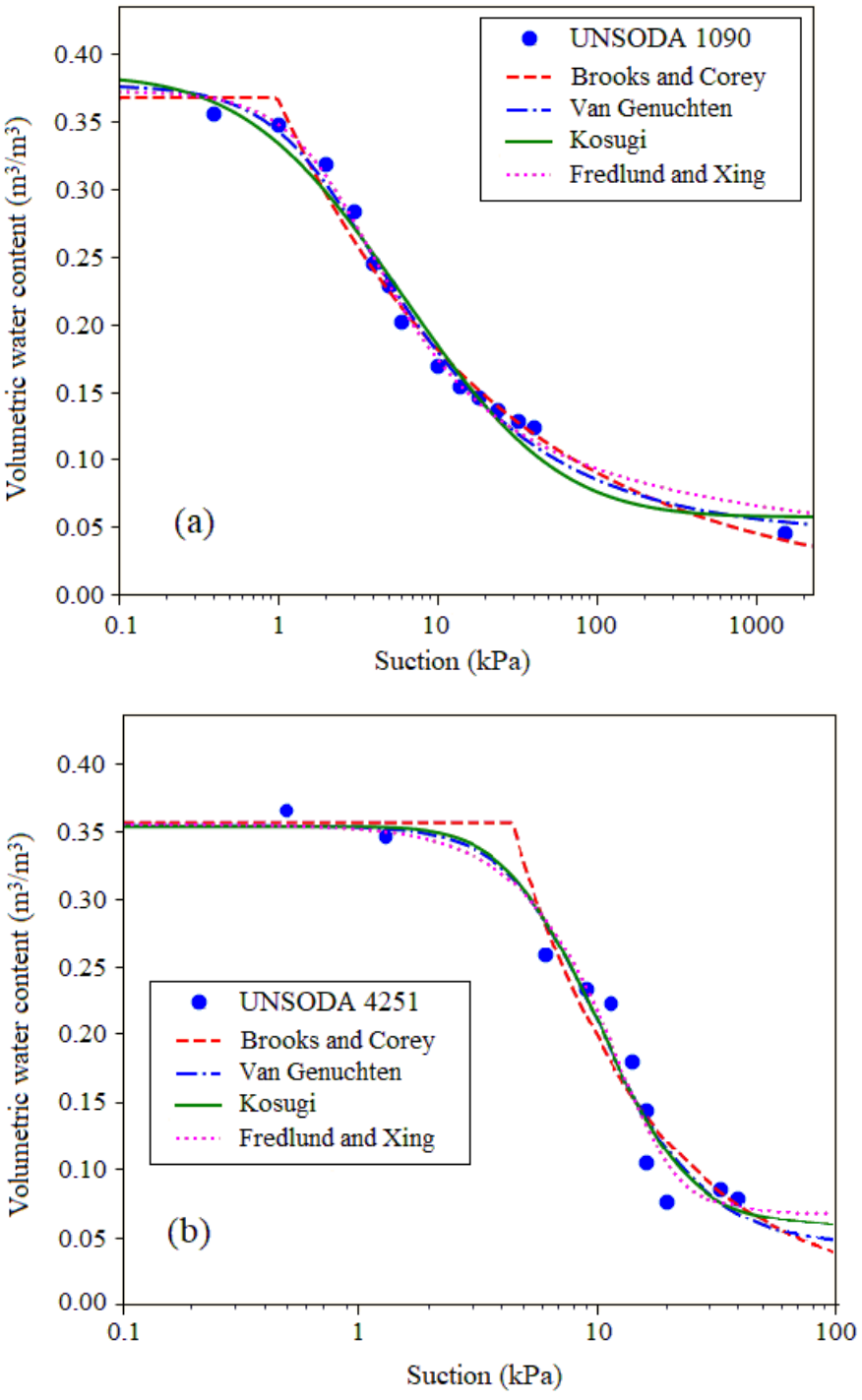

Figure 5. SWCC based on (a) UNSODA 1090 (b) UNSODA 4251

SWCC estimates are based on the UNSODA code. It is the database from Brooks and Corey [20], Van Genuchten [21], Kosugi [22], and Fredlund & Xing [23], which were models for selecting parameters according to Table 3, were compared with the actual measured values and were highly similar. As shown in Figure 5, despite seeing the graphs of all four models showing the same trend, they each give different parameters. However, referring to the use of this UNSODA database, it is possible to choose another parameter to estimate the hydraulic conductivity functions (k-permeability functions) as well [24].

Table 3. Fitting parameters from SWRC

Model	Equation	Top position	Middle and bottom positions
Brooks & Corey (1964)	$\left(\frac{\Psi_a}{\Psi}\right)^{\lambda} = \frac{\theta - \theta_r}{\theta_s - \theta_r}$	θ_S = 36090	θ_S = 35938
		θ_r = 0.032394	θ_r = 0.63×10^{-7}
		h_m=14.482	h_m=23.837
		θ_S = 36090	λ = 0.45431
		λ = 0.42121	θ_S = 35938
Van Genuchten (1980)	$\frac{\theta - \theta_r}{\theta_s - \theta_r} = \left(\frac{1}{1 + (\alpha\Psi)^n}\right)^m$	θ_S = 0.37695	θ_S = 0.35337
		θ_r = 0.043556	θ_r = 0.037314
		α = 0.050997	α = 0.012482
		n = 1.5307	n = 2.4590
Kosugi (1994)	$\theta = \theta_s \left[\frac{\ln\left(\frac{h}{h_m}\right)}{\sigma}\right]$	θ_S = 0.38430	θ_S = 0.35281
		θ_r = 0.057127	θ_r = 0.061369
		h_m=61.502	h_m=103.29
		σ = 1.7689	σ = 0.71862
Fredlund & Xing (1994)	$\theta = \theta_s \left[\frac{1}{\ln\left[e + \left(\frac{\Psi}{\Psi_a}\right)^n\right]}\right]^m$	θ_S = 0.37695	θ_S = 0.35444
		θ_r = 0.31268×10^{-4}	θ_r = 0.74140
		a = 21.634	a = 4415.9
		n=0.83049	n=1247.5
		m= 1.4253	m = 1.7284

4. Analysis

In this analysis, the model was determined by surveying the slopes on which the disaster occurred, as shown in Figure 6, with the characteristics of the top layer of soil being 3 m thick, decomposite rock 1 m thick, and the deepest bedrock. For soil examples, three groups of disaster sites—top, middle, and bottom—are silty sand. Compared with the UNSODA data (Table 2), as described above, in determining the model that is interested in the SWCC properties of the location soil, the middle and lower positions, which are similar in appearance, are therefore both UNSODA 4251, while the top position is UNSODA 1090.

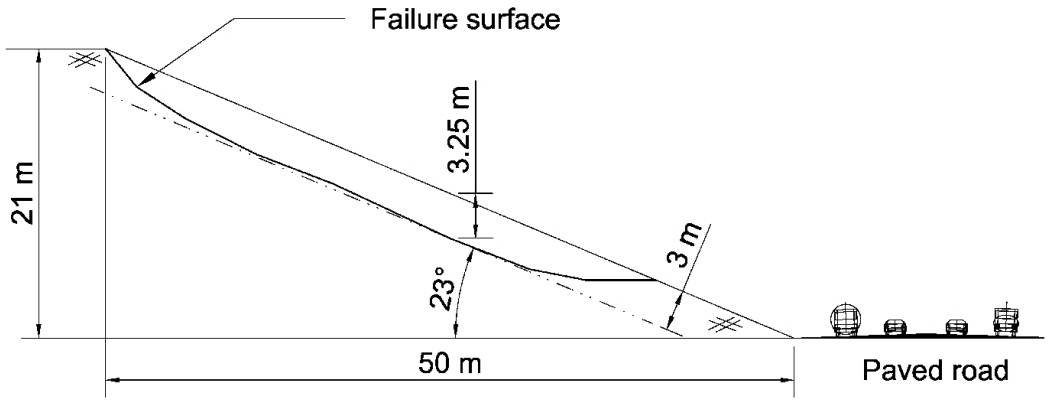

Figure 6. Schematic of studied slope and location of failure surface

Figure 7 shows soil material properties determination in a SEEP/W program using SWCC from UNSODA 1090 and 4251 data to determine the hydraulic conductivity function properties as estimated by the Fredlund and Xing equations (1994) [23]. Flux boundary stabilizers are used to determine the initial state of the pore water pressure on the slope. For the lower and upper vertical bed boundaries, conditions (a-i-h) are defined as no seepage through the base of the soil slope. Likewise, the toe surface (d-e) is a well-compacted, well-paved road. determines that there is no flow. The lower vertical boundary of the section (e-f-g) was defined as the unit gradient (i), while the upper surface conditions (a-b-c-d) were defined as the rainfall intensity (I_r) during the steady-state analysis, as rainfall by the average during November 2021 was specified as a flow rate of 2.42×10^{-7} m/s (627 mm/month), but the transient analysis used daily rainfall for the period from October 2021 to December 2021

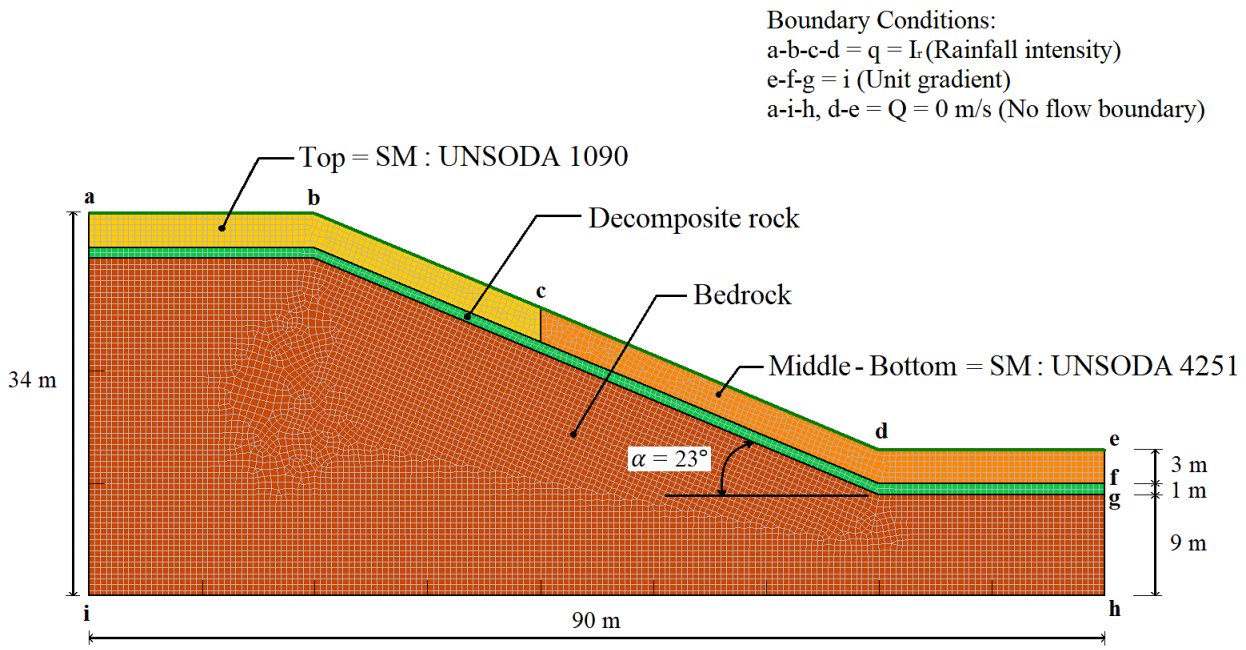

Figure 7. Finite element mesh and boundary conditions

The initial condition of the phreatic surface, which indicates more water accumulated down the slope toe, is shown in Figure 8-a. Following the establishment of the starting condition, a transient analysis was carried out, utilizing the upper flux boundary condition of the recorded daily rainfall episodes from October 2021 to December 2021. These were used as data for the analysis. This is to show the changes before the disaster and after the disaster. The calculated SEEP/W water pressure was used in SLOPE/W, limiting the use of the equilibrium method to calculate the safety factor of the slope. For unsaturated flow, follow the modified Darcy law differential equations for two-dimensional transient water. The flow used in the SEEP/W model is as follows.

$$\frac{\partial}{\partial x}\left(k_x \frac{\partial H}{\partial x}\right) + \frac{\partial}{\partial y}\left(k_y \frac{\partial H}{\partial y}\right) + Q = \frac{\partial \theta}{\partial t} \quad (1)$$

where H is the total head, k_x is hydraulic conductivity in the x direction, k_y is hydraulic conductivity in the y direction, Q is the applied boundary flux, $\frac{\partial \theta}{\partial t}$ is the volumetric water content, t: the time.

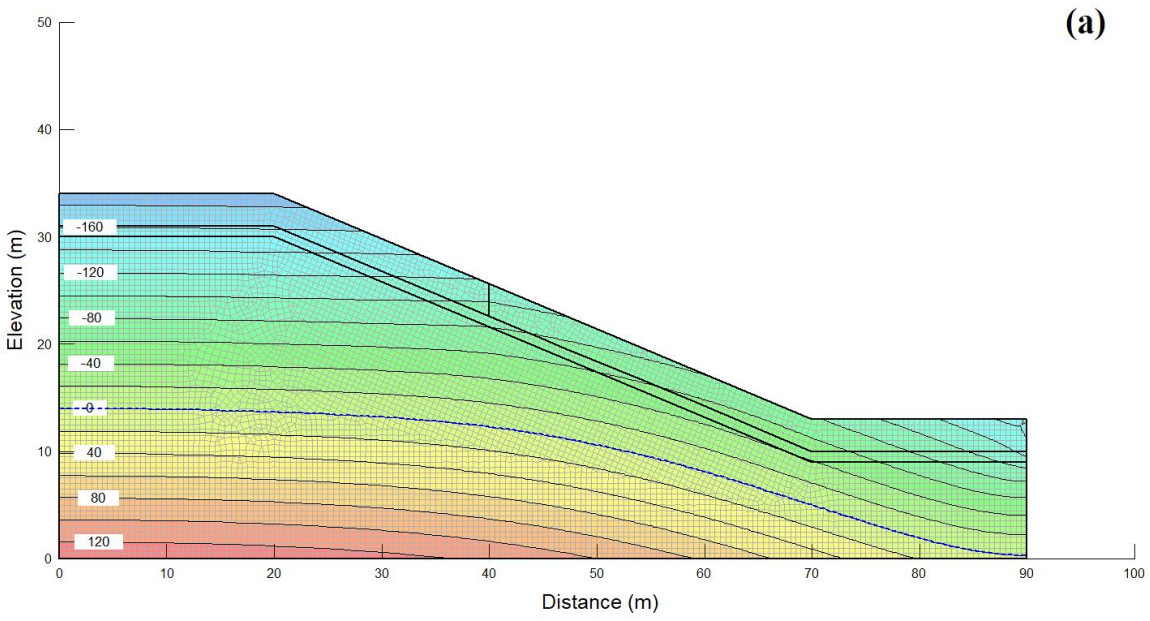

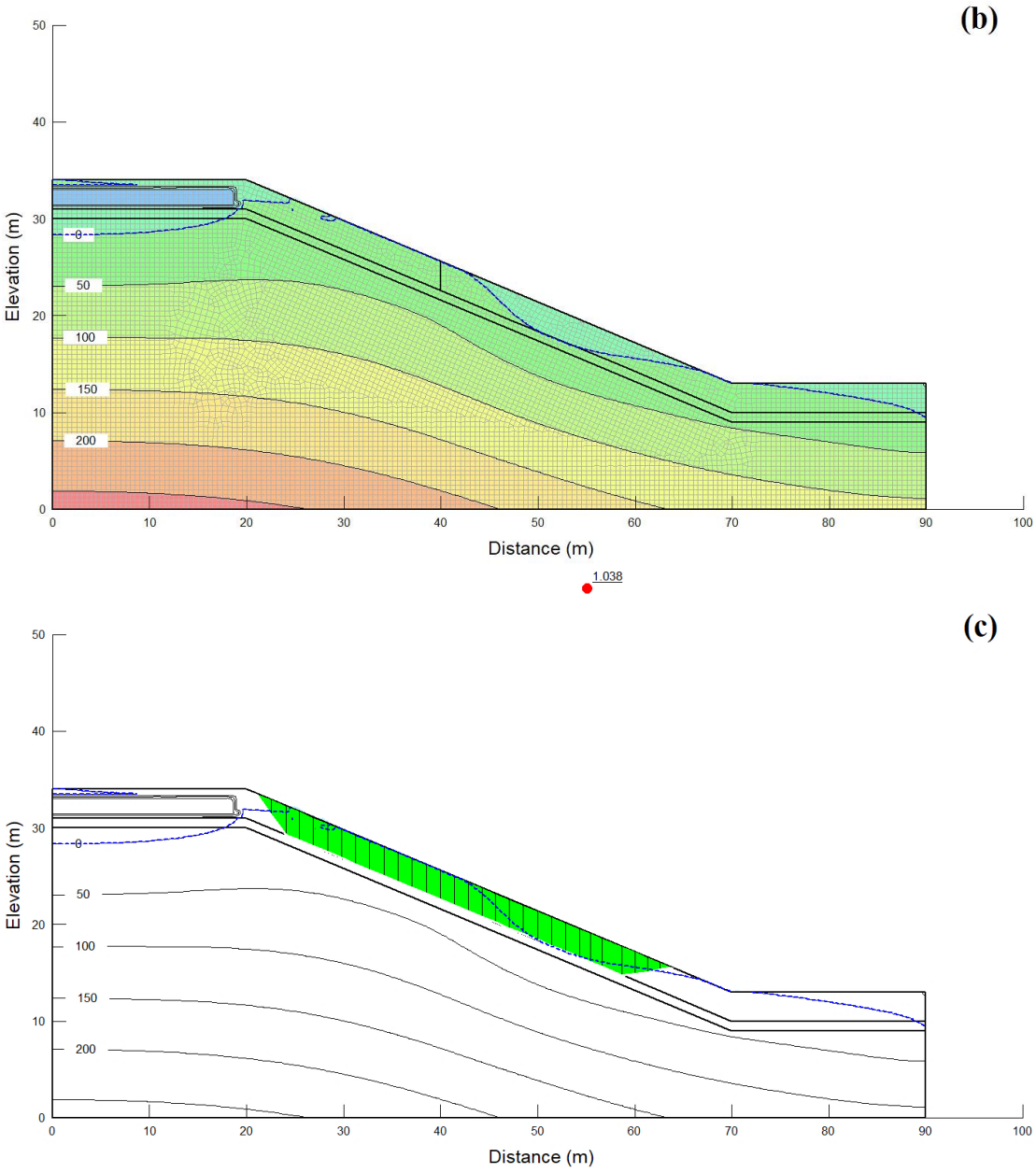

Figure 8. Seepage analysis and stability analysis

The change with pore water pressure during the precipitation received from the transient water seepage analysis using SEEP/W was exported. After that, go to the calculation of SLOPE/W to calculate the slope stability. Unsaturated Shear Equation by Extended Mohr-Coulomb the criteria, the ones used in SLOPE/W, are as follows Fredlund et al. [25].

$$\tau = c' + (\sigma_n - u_a)\tan\phi + (u_a - u_w)\tan\phi^b \quad (2)$$

where τ is the shear strength of the unsaturated soil, c' :the effective cohesion, ϕ is the effective angle of internal friction, $(\sigma_n - u_a)$ is the effective normal stress on the plane of failure, $(u_a - u_w)$ is the matric suction on the plane of failure, ϕ^b is the angle of friction with respect to matric suction in the unsaturated soil. Figures 8-b and 8-c depict changes in pore water pressure predicted by SEEP/W modeling over time, whereas SLOPE/W modeling has the factor of safety = 1.0, which failed on November 18, 2021.

5. Results and Discussion

The authors have tried to find better methods of landslide early warning for a large community building and roadway on a mountain slope near the sea, Khanom, Southern Thailand. As indicated above, a typical geometry of the unsaturated Khanom soil slope was earlier shown in Figure 6. The SWCC plays an essential role in reflecting the hydraulic characteristics of unsaturated soil [26-28]. The permeability parameters acquired from the comparison between grain size distribution data and unsaturated soil hydraulic database (UNSODA) were significant on the infiltration characteristics of the soil. Fredlund & Xing (1994) [23] equation was adopted for the derivation of the SWCC and hydraulic conductivity equations due to its simplicity. Rainfall intensities from monthly rainfall measures were used in the FEM program to compute the factor of safety in the unsaturated soil slope.

The stability analysis results were computed using SEEP/W to model fluctuations in pore-water pressure during rainfall and compute water infiltration rates as surface boundary conditions. Then, stability analysis results computed using SLOPE/W were plotted for a relationship between the time period and the factor of safety (Figure 9). At the site, rainfall infiltrates through the soil, leading to a reduction in matric suction [1] and the safety factor. As shown in Figure 9, there was no heavy rain in October 2021, and the factor of safety with UNSODA data was about 1.2. Then, rainfall intensities increased in mid-November, and we observed a decline in the safety factor from 1.2 to 1.0 on November 18, 2021, which corresponds to the landslide disaster.

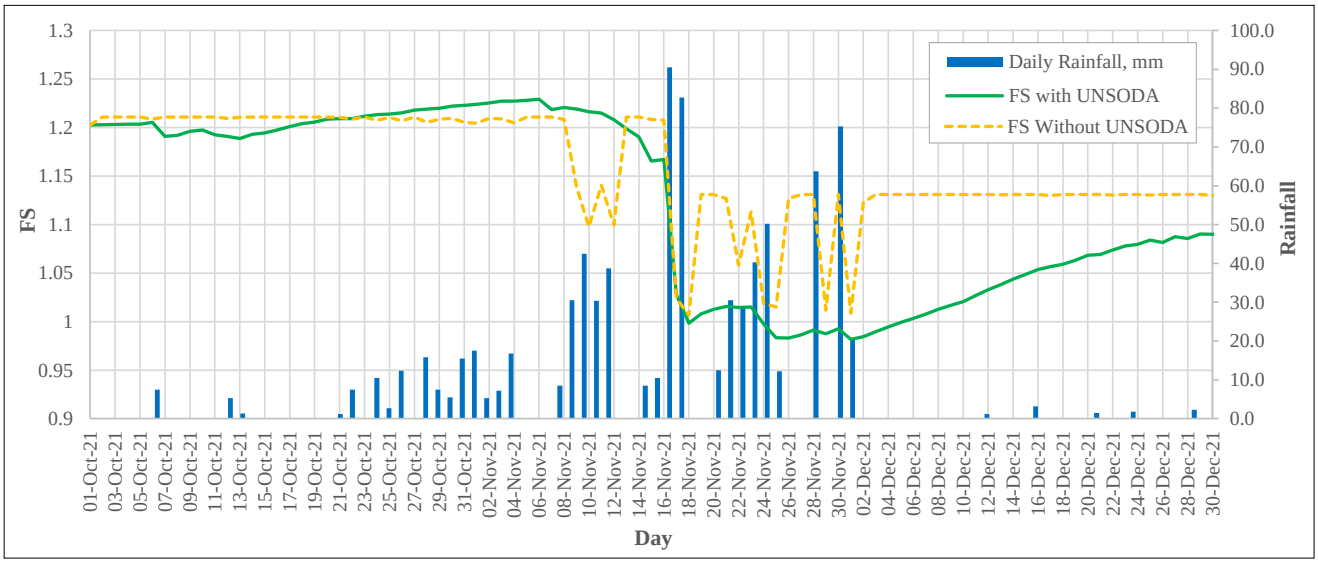

Figure 9. Rainfall versus factor of safety

In unsaturated soil, the permeability parameters are significant for the infiltration characteristics of the soil [12, 19, 29]. Thus, in the case of not using UNSODA data, the rainfall infiltrated through the soil on October 6, 2021, and did not affect the safety factor. While the case of using UNSODA data, the safety factor slightly decreased from 1.2 to 1.18. In addition, there was no rainfall in December 2021, so the value of F.S. without UNSODA will increase immediately, but the factor of safety with UNSODA will gradually increase from 0.98 to 1.08, agreeing well with the behavior of rainfall-induced landslides [30]. The above findings suggested that the slope stability analysis with UNSODA could well be used as an index for landslide early warning.

Furthermore, considering the 3-day cumulative rainfall, which is an analysis based on the Antecedent Precipitation Index value (API) principle of Linsley et al. [31], it was found that on the day of the disaster, and similarly to Okada [32], the cumulative rainfall was more than 200 mm, as shown in Figure 10. This is consistent with the results of past studies (e.g., Soralump [33], Mairaing et al. [34], Jotisankasa et al. [35]) that suggest landslide risk areas in Thailand. Use the alarm threshold from the correlation effect of the rainfall pattern that triggered the failure graph, which is the relationship between the 24-hour rainfall and the 3-day antecedent rainfall.

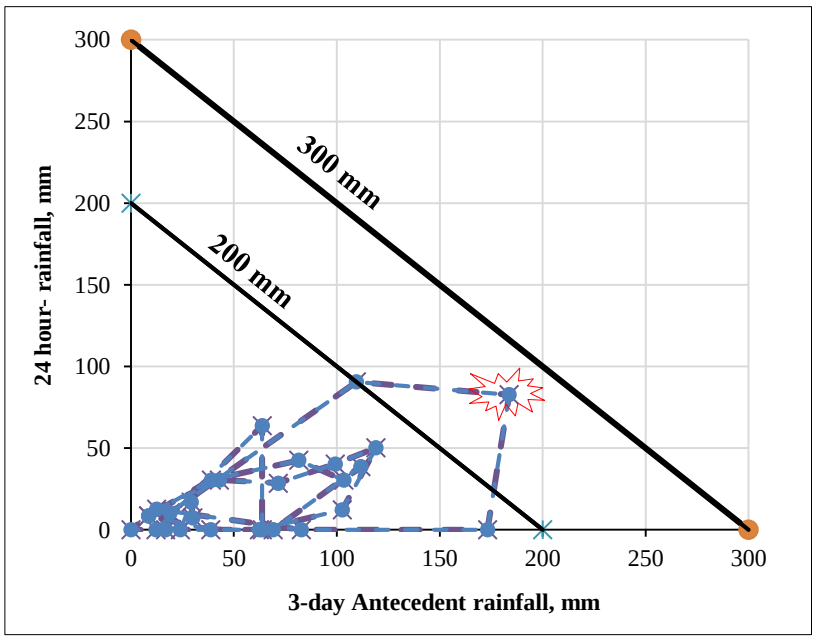

Figure 10. Rainfall pattern that triggered failure in November 2021

6. Conclusion

In slope stability analysis at Khanom in southern Thailand, the area's geology from the traditional survey was used as input parameters. The comparison between soil sampling and the unsaturated soil hydraulic database (UNSODA) was adopted to derive the SWCC equations due to its simplicity. Monthly rainfall measurements were used in the SEEP/W and SLOPE/W programs to compute the variability in pore-water pressure and the factor of safety (F.S.) in the soil slope. The rainfall infiltration process in an unsaturated soil mass led to a reduction of soil strength and the safety factor. The results showed that the F.S. with UNSODA data value was about 1.2. From October 2021 to early November 2021. Then, the soil slope at the site became unstable at F.S. = 1, which corresponds to the data from the landslide disaster on November 18, 2021. Furthermore, this study concludes that the 3-day antecedent rainfall criteria can be utilized as an early warning.

As described, this study aimed to present the advantages of slope stability analysis with the UNSODA hydraulic database. The results from GeoStudio showed that without UNSODA, the safety factor on the event day was higher than 1.0. It shows that the absence of unsaturated soil properties would adversely affect the safety factor assessment, which may miss the alarm. Geotechnical engineers in areas at risk of disasters from heavy rainfall need to assess the risk when working with slopes. Design engineers need to know the permeability parameters and rainfall intensity, including being able to predict landslides more accurately in advance.

7. Declarations

7.1. Author Contributions

Conceptualization, K.M. and C.K.; methodology, C.K.; software, K.M.; validation, K.M. and C.K.; formal analysis, K.M.; investigation, C.K.; resources, C.K.; data curation, K.M.; writing—original draft preparation, C.K.; writing—review and editing, K.M.; visualization, C.K.; supervision, K.M.; project administration, C.K.; funding acquisition, C.K. All authors have read and agreed to the published version of the manuscript.

7.2. Data Availability Statement

The data presented in this study are available on request from the corresponding author

7.3. Funding

This research was financially supported by the Research Unit of Technology and Innovation on Civil Engineering (RICE), Rajamangala University of Technology Srivijaya and Southern Natural Disaster Research Center (NadRec), Prince of Songkhla University for having provided a very helpful information and improving the use of English in the manuscript.

7.4. Acknowledgements

This paper was supported by the Research Unit of Technology and Innovation on Civil Engineering (RICE), Rajamangala University of Technology Srivijaya, for providing beneficial information and improving the use of English in the manuscript.

7.5. Conflicts of Interest

The authors declare no conflict of interest.

8. References

[1] Salee, R., Chinkulkijniwat, A., Yubonchit, S., Horpibulsuk, S., Wangfaoklang, C., & Soisompong, S. (2022). New threshold for landslide warning in the southern part of Thailand integrates cumulative rainfall with event rainfall depth-duration. Natural Hazards, 113(1), 125–141. doi:10.1007/s11069-022-05292-0.

[2] Yang, H., Wei, F., Ma, Z., Guo, H., Su, P., & Zhang, S. (2020). Rainfall threshold for landslide activity in Dazhou, southwest China. Landslides, 17(1), 61–77. doi:10.1007/s10346-019-01270-z.

[3] Kardani, N., Zhou, A., Nazem, M., & Shen, S. L. (2021). Improved prediction of slope stability using a hybrid stacking ensemble method based on finite element analysis and field data. Journal of Rock Mechanics and Geotechnical Engineering, 13(1), 188–201. doi:10.1016/j.jrmge.2020.05.011.

[4] Zheng, Q., Lyu, H. M., Zhou, A., & Shen, S. L. (2021). Risk assessment of geohazards along Cheng-Kun railway using fuzzy AHP incorporated into GIS. Geomatics, Natural Hazards and Risk, 12(1), 1508–1531. doi:10.1080/19475705.2021.1933614.

[5] Segoni, S., Piciullo, L., & Gariano, S. L. (2018). A review of the recent literature on rainfall thresholds for landslide occurrence. Landslides, 15(8), 1483–1501. doi:10.1007/s10346-018-0966-4.

[6] Teja, T. S., Dikshit, A., & Satyam, N. (2019). Determination of rainfall thresholds for landslide prediction using an algorithm-based approach: Case study in the Darjeeling Himalayas, India. Geosciences (Switzerland), 9(7), 302. doi:10.3390/geosciences9070302.

[7] Zhao, Y., Meng, X., Qi, T., Qing, F., Xiong, M., Li, Y., Guo, P., & Chen, G. (2020). AI-based identification of low-frequency debris flow catchments in the Bailong River basin, China. Geomorphology, 359, 107125. doi:10.1016/j.geomorph.2020.107125.

[8] Jiang, Z., Fan, X., Siva Subramanian, S., Yang, F., Tang, R., Xu, Q., & Huang, R. (2021). Probabilistic rainfall thresholds for debris flows occurred after the Wenchuan earthquake using a Bayesian technique. Engineering Geology, 280, 105965. doi:10.1016/j.enggeo.2020.105965.

[9] Chen, Y., Hu, R., Zhou, C., Li, D., & Rong, G. (2011). A new parabolic variational inequality formulation of Signorini's condition for non-steady seepage problems with complex seepage control systems. International Journal for Numerical and Analytical Methods in Geomechanics, 35(9), 1034–1058. doi:10.1002/nag.944.

[10] Liu, W., Luo, X., Huang, F., & Fu, M. (2017). Uncertainty of the soil-water characteristic curve and its effects on slope seepage and stability analysis under conditions of rainfall using the Markov chain Monte Carlo method. Water (Switzerland), 9(10), 758. doi:10.3390/w9100758.

[11] Hamdany, A. H., Shen, Y., Satyanaga, A., Rahardjo, H., Lee, T. T. D., & Nong, X. (2022). Field instrumentation for real-time measurement of soil-water characteristic curve. International Soil and Water Conservation Research, 10(4), 586–596. doi:10.1016/j.iswcr.2022.01.007.

[12] Wang, L., Tang, L., Wang, Z., Liu, H., & Zhang, W. (2020). Probabilistic characterization of the soil-water retention curve and hydraulic conductivity and its application to slope reliability analysis. Computers and Geotechnics, 121, 103460. doi:10.1016/j.compgeo.2020.103460.

[13] Dafalla, M. A., Al-Mahbashi, A. M., Almajed, A., & Al-Shamrani, M. (2020). Predicting Soil-Water Characteristic Curves of Clayey Sand Soils Using Area Computation. Mathematical Problems in Engineering, 2020(4548912). doi:10.1155/2020/4548912.

[14] Wang, Z., Li, X., Shi, H., Li, W., Yang, W., & Qin, Y. (2020). Estimating the water characteristic curve for soil containing residual plastic film based on an improved pore-size distribution. Geoderma, 370, 114341. doi:10.1016/j.geoderma.2020.114341.

[15] Zhou, J., Ren, J., & Li, Z. (2021). An Improved Prediction Method of Soil-Water Characteristic Curve by Geometrical Derivation and Empirical Equation. Mathematical Problems in Engineering, 2021(9956824). doi:10.1155/2021/9956824.

[16] Zhou, W. H., Yuen, K. V., & Tan, F. (2014). Estimation of soil-water characteristic curve and relative permeability for granular soils with different initial dry densities. Engineering Geology, 179, 1–9. doi:10.1016/j.enggeo.2014.06.013.

[17] Minasny, B., McBratney, A. B., & Bristow, K. L. (1999). Comparison of different approaches to the development of pedotransfer functions for water-retention curves. Geoderma, 93(3–4), 225–253. doi:10.1016/S0016-7061(99)00061-0.

[18] Chiu, C. F., Yan, W. M., & Yuen, K. V. (2012). Estimation of water retention curve of granular soils from particle-size distribution - a Bayesian probabilistic approach. Canadian Geotechnical Journal, 49(9), 1024–1035. doi:10.1139/T2012-062.

[19] Wang, L., Zhang, W., & Chen, F. (2019). Bayesian approach for predicting soil-water characteristic curve from particle-size distribution data. Energies, 14(15), 2992. doi:10.3390/en12152992.

[20] Brooks, R. H., & Corey, A. T. (1964). Hydraulic Properties of Porous Media and Their Relation to Drainage Design. Transactions of the ASAE, 7(1), 0026–0028. doi:10.13031/2013.40684.

[21] Van Genuchten, M. T. (1980). A Closed-form Equation for Predicting the Hydraulic Conductivity of Unsaturated Soils. Soil Science Society of America Journal, 44(5), 892–898. doi:10.2136/sssaj1980.03615995004400050002x.

[22] Kosugi, K. (1994). Three-parameter lognormal distribution model for soil water retention. Water Resources Research, 30(4), 891–901. doi:10.1029/93WR02931.

[23] Fredlund, D. G., & Xing, A. (1994). Equations for the soil-water characteristic curve. Canadian Geotechnical Journal, 31(4), 521–532. doi:10.1139/t94-061.

[24] Kosugi, K. (1999). General Model for Unsaturated Hydraulic Conductivity for Soils with Lognormal Pore-Size Distribution. Soil Science Society of America Journal, 63(2), 270–277. doi:10.2136/sssaj1999.03615995006300020003x.

[25] Fredlund, D. G., Morgenstern, N. R., & Widger, R. A. (1978). Shear Strength of Unsaturated Soils. Canadian Geotechnical Journal, 15(3), 313–321. doi:10.1139/t78-029.

[26] Liu, Y., Tian, G., Wang, S., Satyanaga, A., & Zhai, Q. (2022). Parametric Analysis of Rainfall-Induced Loess Soil Slope Due to the Rainwater Infiltration. Urban Science, 6(3), 54. doi:10.3390/urbansci6030054.

[27] Das, P., Patwa, D., Vishnu, G., & Bharat, T. V. (2022). Influencing factors on the simulation of rainfall-induced landslide prediction based on case study. Bulletin of Engineering Geology and the Environment, 81(5), 194. doi:10.1007/s10064-022-02682-3.

[28] Zhang, Z., Fu, X., Sheng, Q., Du, Y., Zhou, Y., & Huang, J. (2021). Stability of Cracking Deposit Slope Considering Parameter Deterioration Subjected to Rainfall. International Journal of Geomechanics, 21(7), 5021001. doi:10.1061/(asce)gm.1943-5622.0002045.

[29] Wang, C., Li, S., He, X., Chen, Q., Zhang, H., & Liu, X. (2021). Improved prediction of water retention characteristic based on soil gradation and clay fraction. Geoderma, 404, 115293. doi:10.1016/j.geoderma.2021.115293.

[30] Kanjanakul, C., Chub-uppakarn, T., & Chalermyanont, T. (2016). Rainfall thresholds for landslide early warning system in Nakhon Si Thammarat. Arabian Journal of Geosciences, 9(11), 584. doi:10.1007/s12517-016-2614-4.

[31] Linsley, R. K., Kohler, M. A., & Paulhus, J. L. H. (1982). Hydrology for engineers (3rd Ed.). McGraw-Hill Book Company, New York. United States.

[32] Okada, K., Sugiyama, T., Muraishi, H., Noguchi, T., & Samizo, M. (1994). Statistical risk estimating method for rainfall on surface collapse of cut slope. Soils and Foundations, 34(3), 49–58. doi:10.3208/sandf1972.34.3_49.

[33] Soralump, S. (2010). Rainfall-triggered landslide: from research to mitigation practice in Thailand. Geotechnical Engineering, 41(1), 1-39.

[34] Mairaing, W., Jotisankasa, A., & Soralump, S. (2012). Some applications of unsaturated soil mechanics in Thailand: an appropriate technology approach. Geotechnical Engineering Journal of the SEAGS & AGSSEA, 43(1), 1-11.

[35] Jotisankasa, A., Mahannopkul, K., & Sawangsuriya, A. (2015). Slope stability and pore-water pressure regime in response to rainfall: A case study of granitic fill slope in northern Thailand. Geotechnical Engineering Journal of the SEAGS & AGSSEA, 46(1), 45-54.